Flight path optimization for noise reduction in the vicinity of airports

André. S. Sousa

Instituto Superior Técnico, University of Lisbon, Av. Rovisco Pais, 1049-001 Lisbon, Portugal

Abstract

In recent years, aviation noise has become a growing concern. Due to an expected increase of commercial air traffic, accompanied by an amplified public environmental awareness, aviation regulators are now required to review existing legislation and demand to both aircraft manufacturers and operators the commitment to noise reduction campaigns in their fields of activity. These policies lead to the development of increasingly accurate noise prediction tools that include more complex sound propagation models and that simultaneously allow real-time computations in an operational environment.

This dissertation presents a model adequate for sound propagation over a flat surface with realistic atmospheric conditions. The model is a hybrid combination of two physics-based sound propagation schemes: the parabolic equation and the ray model.

As the program developed in this thesis is oriented towards aviation noise, a method of defining the aircraft power spectrum was adopted and several empirical correlations were included in order to model source directivity. With this procedure, the hybrid model may represent complex sound sources moving along specified flight paths.

The numerical methods were validated using benchmark test cases created for different meteorological environments. The program was applied to different airport scenarios by resorting to realistic flight parameters and the coherent results obtained confirmed the suitability of the hybrid model to study aircraft noise in the vicinity of airports.

Keywords: sound propagation, aviation noise, hybrid model, noise reduction.

1 Introduction

For communities established in the vicinity of airports, aviation noise has become a major concern as the regular operation of multiple aircraft can become an unwelcome presence.

Although aircraft are becoming quieter, due to the forecasts of continuous air traffic growth (International Civil Aviation Organization, 2010) and increased public awareness to the health issues brought by aircraft noise, these concerns are becoming more important than ever and it is expected that they continue to drive both commercial and military operations.

Following the directives of aviation authorities, several computational applications have been developed by national regulators in order to predict noise contours in major airports that can help to minimize the impact of aviation noise by providing tools that facilitate land use management and that offer a direct approach to mitigate noise influence in specific areas. For these reasons, viable numerical models must be employed in order to produce accurate results regarding noise propagation in the atmosphere.

Using two accepted propagation models, the Green's Function Parabolic Equation (GFPE) method and the ray model, we developed a hybrid propagation model in Matlab. This algorithm is combined with the definition of aircraft as complex noise sources by applying a reverse engineering process to published experimental data. This program is well suited for noise prediction in airports as it is capable of translating in-flight parameters to quantities relevant for the noise propagation algorithms.

2 The GFPE Method

2.1 Theoretical formulation

As in previous derivations, we consider a monopole source located above a finite impedance flat ground surface, in an atmosphere with a non constant sound speed profile. Similarly to the majority of sound prediction programs, the application presented in this text assumes that the system exhibits azimuthal symmetry about the vertical axis z. This assumption allows a two-dimensional representation of the atmosphere by resorting to an approximation of the three--dimensional Helmholtz equation.

Removing the cylindrical spreading by introducing a variable $q_c = p_c\sqrt{r}$ and assuming valid the far-field approximation, the two-dimensional version of the Helmholtz equation becomes

$$\frac{\partial^2 q}{\partial r^2} + \frac{\partial^2 q}{\partial z^2} + k^2 q = 0, \qquad (1)$$

where $k(z) = \omega/c(z)$ is the wave number, ω is the angular frequency and $c(z)$ is the speed of sound. The derivation of the general GFPE method is based on the two-dimensional Kirchhoff-Helmholtz integral equation. The result is the Rayleigh integral for the field $q(\boldsymbol{R})$ at a location $\boldsymbol{R_1}$, which is evaluated over a vertical line at a range $r = r_0$. Considering these conditions, the Rayleigh integral is

$$q(\boldsymbol{R_1}) = \frac{1}{2\pi}\int_0^\infty \left(q(\boldsymbol{R}) \frac{\partial g(\boldsymbol{R};\boldsymbol{R_1})}{\partial r} \right) dz, \qquad (2)$$

being $\boldsymbol{R_1} = (r_1, z_1)$ and $\boldsymbol{R} = (r, z)$.

The two-dimensional Green's function $g(\boldsymbol{R};\boldsymbol{R_1})$ also satisfies the two-dimensional Helmholtz equation and it is written as

$$[\partial_r^2 + \partial_z^2 + k^2] g(\boldsymbol{R};\boldsymbol{R_1}) = 4\pi\delta(\boldsymbol{R} - \boldsymbol{R_1}), \qquad (3)$$

where it is assumed that the wave number k is a function of z only, so that the range dependence of the wave number is modeled by changing its value between successive horizontal steps. Consequently, the Green's function can be expressed as $g(\Delta r, z, z_1)$, where $\Delta r = r_1 - r$ is the horizontal spacing. To write the Green's function with relation to the horizontal wave number k_h, the following Fourier transform is introduced

$$G(k_h, z, z_1) = \int_{-\infty}^{+\infty} g(\Delta r, z, z_1) e^{-ik_h \Delta r}\, d(\Delta r). \qquad (4)$$

The inverse Fourier transform is expressed by the following equation:

$$g(\Delta r, z, z_1) = \frac{1}{2\pi}\int_{-\infty}^{+\infty} G(k_h, z, z_1) e^{ik_h \Delta r}\, dk_h. \qquad (5)$$

Considering the Fourier transform properties, substitution of equation (5) into equation (2) gives (changing the notation from z_1 to z and from z to z')

$$q(r + \Delta r, z) = \frac{1}{4\pi^2 i}\int_{-\infty}^{+\infty} k_h e^{ik_h \Delta r}\, dk_h \times \int_0^\infty G(k_h, z', z) q(r, z')\, dz'. \qquad (6)$$

The Green's function $G(k_h, z', z)$ satisfies the Fourier transformed variant of equation (3) and it is written as

$$[\partial_z^2 + k^2(z) - k_h^2] G(k_h, z', z) = -4\pi\delta(z - z'). \qquad (7)$$

Resorting to equation (6), the following expression is obtained for a refracting atmosphere

$$\psi(r + \Delta r, z) = e^{i\Delta r \frac{\delta k^2(z)}{2k_a}} \times \left\{ \frac{1}{2\pi}\int_{-\infty}^{+\infty} [\Psi(r, k_z) + R(k_z)\Psi(r, -k_z)] e^{i\Delta r\left(\sqrt{k_a^2 - k_z^2} - k_a\right)} e^{ik_z z} dk_z + 2i\beta\Psi(r, \beta) e^{-i\beta z} e^{i\Delta r\left(\sqrt{k_a^2 - \beta^2} - k_a\right)} \right\}, \qquad (8)$$

where

$$\Psi(r,k_z)=\int_0^{\infty} e^{-ik_z z'}\psi(r,z')\,dz' \qquad (9)$$

is the spatial Fourier Transform of the pressure field $\psi(r,z)=e^{-ik_a r}q(r,z)$.

In equation (8), Δr is the horizontal spacing, k_a is a reference wave number and $\beta=k_0/Z_g$. The plane wave reflection coefficient is written as $R(k_z)=\left(k_z Z_g-k_0\right)/\left(k_z Z_g+k_0\right)$, where Z_g is the ground impedance and k_0 is the wave number at zero height.

The atmospheric refraction is included in equation (8) by multiplying the solution of a homogeneous atmosphere by the exponential factor $exp[i\Delta r\,\delta k^2(z)/(2k_a)]$, where the term $\delta k^2(z)$ is defined as follows

$$k^2(z)=k_a^2+\delta k^2(z). \qquad (10)$$

2.2 Numerical formulation

As the GFPE method is a step by step extrapolation of the sound field $\psi(r+\Delta r,z)$, a two dimensional rectangular grid is used, where the two grid parameters (horizontal spacing Δr and vertical spacing Δz) are frequency dependent. The length of the numerical grid is defined as the number of horizontal steps necessary to reproduce the horizontal distance between the source and the receiver. Simultaneously, the grid is limited by the ground surface at $z=0$ and by a top height $z_{top}=M\Delta z$, where M is a positive integer dependent on the source height. To prevent unrealistic wave reflections at the top of the numerical grid, an attenuation layer is located between $z=z_{abs}$ and $z=z_{top}$, where its thickness typically varies between 50λ and 100λ, being λ the average wavelength. This attenuation is obtained by adding an imaginary term to the wave number within the absorption layer, which is defined as

$$\alpha(z)=A\left(\frac{z-z_{abs}}{z_{top}-z_{abs}}\right)^2, \qquad (11)$$

where A is a frequency dependent parameter.

To allow a correct comparison with benchmark results, we adopted a fourth order Gaussian starting field that is written as

$$q_o(0,z)=\sqrt{ik_a}\times \left(A_0+A_2k_a^2z^2+A_4k_a^4z^4+A_6k_a^6z^6+A_8k_a^8z^8\right)e^{-\frac{k_a^2z^2}{B}}, \qquad (12)$$

being the coefficients A_i and B determined by the order of the starting field (Salomons, 2001). To include the influence of a ground surface, equation (12) is modified as follows

$$q(0,z)=q_0(z-z_s)+\frac{Z_g-1}{Z_g+1}q_0(z+z_s), \qquad (13)$$

where z_s is the source height.

To calculate the sound field it is necessary to compute multiple Fourier integrals in each extrapolation step. Consequently, each integral is approximated by a discrete sum named Discrete Fourier Transform (DFT). For the Fourier integral defined in equation (9), we may write the following DFT:

$$\Psi(r,k_z)\approx\left[\sum_{j=0}^{N-1}\psi\left(r,z_j\right)e^{-ik_n z_j}\right]\Delta z, \qquad (14)$$

where the two integration variables are discretized as

$$k_n=n\Delta k,\quad n=0,1,2,\dots,N/2,-N/2+1,-N/2+2,\dots,-1, \qquad (15)$$

$$z_j=j\Delta z,\quad j=0,1,2,\dots,N-1, \qquad (16)$$

being $\Delta k=2\pi/(N\Delta z)$, Δz the vertical spacing of the numerical grid and where $N=2M$ is the Fourier transform size, related to the grid vertical dimension.

As an effect of Fourier transform's periodicity, $\Psi(r,k_z)$ and $\Psi(r,-k_z)$ may be determined with a

single transform of size $N = 2M$ and related by a permutation of vector positions, consequently reducing the overall computational effort. On the other hand, the integral $\Psi(r, \beta)$ is calculated with a single summation of N terms following the definition of a DFT.

Previous studies of the GFPE method's precision have shown that the overall accuracy may be enhanced by using the following exponential factor

$$e^{i\Delta r \delta k(z)} \quad (17)$$

and as a result all the computational simulations discussed in this text use the approach defined in equation (17).

3 The Ray Model

3.1 Theoretical formulation

Outdoor sound propagation may be regarded as the propagation of multiple sound rays emanated from a source across the atmosphere; this approach is called geometrical acoustics.

Consequently, the pressure amplitude at a specified location is given by the sum of the pressure amplitudes of each ray that passes through that position:

$$p_c = \sum_{m=1}^{N_{rays}} A_m e^{i\phi_m}, \quad (18)$$

where A_m and ϕ_m are respectively the amplitude and phase of the m^{th} ray.

The computation of the total pressure at a specific receiver is correlated with the determination of all rays intersecting that location, thus being necessary to follow a procedure called ray tracing. The trajectory followed by a sound ray is obtained from the integration of Snell's law, which is defined as

$$\frac{\cos\gamma}{c} = constant\ along\ a\ sound\ ray, \quad (19)$$

where γ is the angle of the ray's trajectory and $c = c(z)$ is the sound speed at the height where the calculation is done.

Therefore, the trajectory of a sound ray in a homogeneous atmosphere is represented by a straight line while in a refracting atmosphere the sound rays are curved according to the speed gradient along the atmosphere.

3.2 Numerical formulation

As the process of ray tracing may become complex for low elevation angles and long range propagation in refracting atmospheres, we implemented a simplified version called two ray model where only two sound rays are considered, the direct ray and the reflected ray. The two ray model is only valid for large elevation angles, and consequently it can be verified that in its region of validity ray curvature is in practice negligible so an additional approximation is employed, where we consider both rays are modeled as straight rays.

Defining the source position as $(0, z_s)$ and the receiver location by (r, z), the distance travelled by the direct ray is

$$R_1 = \sqrt{r^2 + (z - z_s)^2}. \quad (20)$$

On the other hand, the distance covered by the reflected ray may be calculated considering an imaginary source below the ground source, resulting in the following equation:

$$R_2 = \sqrt{r^2 + (z + z_s)^2}. \quad (21)$$

At last, the determination of the complex pressure amplitude follows the relation given by

$$p_c = S\frac{e^{ikR_1}}{R_1} + R_P S\frac{e^{ikR_2}}{R_2}, \quad (22)$$

being R_P the plane wave reflection coefficient defined as

$$R_P = \frac{Z_g \cos\theta - 1}{Z_g \cos\theta + 1}. \qquad (23)$$

4 Hybrid Model

The GFPE propagation method is well suited for low elevation angles and it is valid for a wide variety of sound frequencies. It can be verified that the maximum elevation angle where accuracy can be attained is mainly due to the choice of an adequate starting field (Cooper and Swanson, 2007), while the other numerical variables have a lower influence on the region of validity. Therefore, it can be shown that a standard Gaussian field (Gilbert and Di, 1993) provides accurate results up to an elevation angle of $35°$, whereas a higher-order starting field (Salomons, 2001) as the one described in section 2.2 returns an accurate pressure field for a maximum angle of approximately $50°$.

On the other hand, the simplified variant of the ray model implemented in this text is employed for high elevation angles, where the number of rays that reach the receiver's position is approximately two and the effects of atmospheric refraction are negligible. For that reason, the lower limit of the validity region of the two ray model is typically imposed at approximately $50°$ (Boeker and Rosenbaum, 2012).

In this text we developed a method that, while preserving a simple implementation in a programming language as the first, merges the sound pressure level obtained in the transition region (L_P) by employing a linear interpolation scheme between the results of the GFPE method $(L_{P,GFPE})$ and the ray model $(L_{P,Ray\ Model})$:

$$L_P = L_{P,GFPE}\frac{\gamma_{top} - \gamma}{\gamma_{top} - \gamma_{bottom}} + L_{P,Ray\ Model}\frac{\gamma - \gamma_{bottom}}{\gamma_{top} - \gamma_{bottom}}, \qquad (24)$$

where γ is the elevation angle and γ_{bottom} and γ_{top} are respectively the lower and upper limits of the merging region. Equation (24) is only valid when the elevation angle γ is within the interval $\gamma_{bottom} \le \gamma \le \gamma_{top}$, otherwise we apply the following criterion

$$L_P = \begin{cases} L_{P,GFPE}, & \gamma < \gamma_{bottom} \\ L_{P,Ray\ Model}, & \gamma > \gamma_{top} \end{cases}. \qquad (25)$$

5 Aircraft as a Noise Source

5.1 Aircraft Power Spectrum

Noise certification plays an important role in an airplane design process. Therefore, several simulations and flight tests must be performed and the results must fulfill the requirements of the International Civil Aviation Organization to guarantee the aircraft's airworthiness. The information regarding each airplane is condensed into one single public database called Aircraft Noise and Performance (ANP) database (Eurocontrol, 2012; International Civil Aviation Organization, 2005) and three different quantities are related: noise level, aircraft thrust setting and distance from the receiver.

The ANP database allows the definition of the power spectrum of each aircraft by employing a reverse engineering method described in detail by Butikofer (2006). Using this process, we were able to obtain the power spectrum for different Airbus models, namely the A319/320/321, A330 and A340 families. The curve obtained from the spreadsheet relates the engine power spectrum with the $1/3$-octave band centre frequencies.

As the determined spectra are only applicable for a limited number of thrust settings, we implemented in the computational application discussed in this text a linear interpolation algorithm for intermediate values (Butikofer, 2006).

5.2 Aircraft Directivity

As aircraft are complex noise emitters, they cannot be modeled as a point source with an omnidirectional sound spreading. Therefore, the determination of the sound field must include

additional correction factors that reflect the effects of lateral and longitudinal directivity. These effects are affected by the relative position between the source and the receiver and are governed by the spherical angles θ and φ, represented in Figure 1.

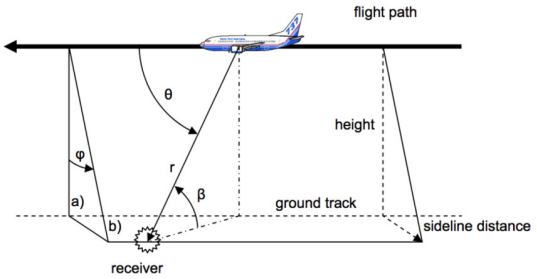

Figure 1 - Aircraft sound emission coordinates (Butikofer, 2006).

Lateral directivity is often called engine installation effect and it reflects the influence of the engine location and type on the overall sound directivity of the aircraft. This effect is directly related to the spherical angle φ. The SAE AIR 5662 (Society of Automotive Engineers, 2006) proposes two expressions that model the lateral effects of engine installation for fuselage mounted engines and wing mounted engines, whereas for propeller driven aircraft there is no correction factor available.

Longitudinal directivity is mostly influenced by the engine characteristics as the bypass ratio and the type of fan installed. Butikofer (2006) provides the value of the correction factor $\Delta L_{longitudinal}$ as a function of the longitudinal angle θ for different classes of aircraft, namely jet powered aircraft (with four different generations of jet engines included), propeller driven vehicles and at last military airplanes.

6 Analysis and Results

6.1 Test cases

This section defines different test cases used to analyze the accuracy of the numerical implementation of the propagation models discussed previously.

The pressure levels are quantified by resorting to either the relative sound pressure level or the transmission loss.

For the validation of the GFPE method, we adopted the cases published by Attenborough et al. (1995), as established in Table 1 and Table 2.

Table 1 - Acoustic parameters for the validation cases of the GFPE method.

Ground Surface	Absorbing
$10\ Hz$	$Z_g = 38.79 + 38.41i$
$100\ Hz$	$Z_g = 12.81 + 11.62i$
$1000\ Hz$	$Z_g = 5.96 + 2.46i$
Source Height (m)	5
Receiver Height (m)	1

The three test cases that allow the validation of the GFPE method consider a homogeneous atmosphere (case 1), a downward refracting environment (case 2) and an upward refracting atmosphere (case 3).

Each of the three test cases presented in the previous paragraph considers a ground surface with a effective flow resistivity of $366\ kPa \cdot s/m^2$, a source height of $5\ m$ and a receiver at $1\ m$ above the ground. The corresponding normalized ground impedances were obtained with a four parameter model using the criteria proposed by Attenborough et al. (1995).

Table 2 - Atmospheric refraction parameters of the test cases for the GFPE method and the ray model validation.

Case	1	2	3	4	5
Speed $c\ (m/s)$	Homogeneous $c = 343$	Downward $c = 343 + z/10$	Upward $c = 343 - z/10$	Homogeneous $c = 343$	Homogeneous $c = 343$

As the two ray model is only valid in a homogeneous atmosphere, where it produces an analytical solution of the wave equation, we adopted two scenarios (case 4 and case 5) proposed by Salomons (2001) (see

Table 2 and Table 3) that allow the comparison of the pressure field evolutions produced by different propagation schemes, namely the GFPE method and the two ray model.

Table 3 - Test conditions for the two ray model validation.

Test Case	4	5
Flow Resistivity $\sigma\ (kPa\ s/m^2)$	200	200
Frequency $f\ (Hz)$	500	300

The first validation test of the ray model (case 4) studies the pressure distribution for multiple receiver positions with constant height. In this simulation, the source is at an height of $2\,m$ and the receiver is $50\,m$ from the ground surface.

On the other hand, test case 5 studies the pressure evolution for multiple receivers lying on a vertical line. The pressure field is calculated assuming the same source position as in the previous case and considering that all observers are at an horizontal distance of $400\,m$ from the source.

The validation process of the hybrid model discussed in this text is based on the atmospheric conditions established for test case 1, where the positions for the receiver and source are defined in Table 4.

Table 4 - Conditions for the validation cases of the transition region.

Test Case	6
Source Height (m)	25
Receiver Height (m)	-
Maximum Range (m)	200

6.2 GFPE validation

The GFPE method was validated using the conditions for test case 1 to 3. To facilitate a comparison with the benchmark data, the results obtained by employing the GFPE model were plotted in a similar structure to the reference results (Attenborough et al., 1995). By comparing the numerical results with the reference data from Attenborough et al.(1995), we concluded that the results were consistent with the benchmark values and the implementation of the GFPE model could be considered valid.

6.3 Ray Model validation

As the implemented GFPE method was validated previously, it can be used as a reference for the validation of the two ray model.

Figure 2 presents the relative SPL as a function of range obtained using both the GFPE scheme and the two ray model in a homogeneous atmosphere. We can verify that both models agree with each other from a range of $20\,m$ up to $100\,m$ and that major differences are only noticeable at the first range steps, up to a range of $20\,m$, as well as in the vicinity of relative SPL minimums.

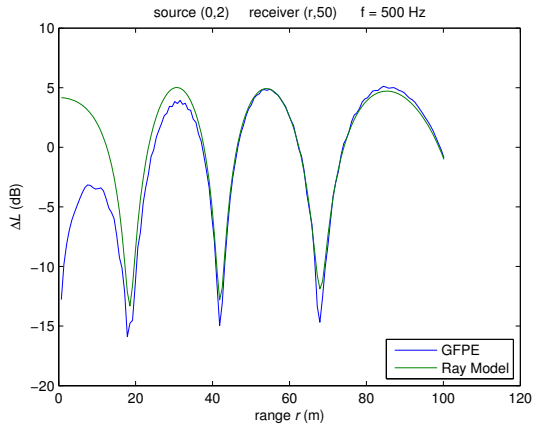

Figure 2 - Relative SPL as a function of range for a receiver height of $50\,m$.

Similar conclusions were obtained by following the conditions specified for test case 5.

The results obtained show that the numerical schemes produce coherent pressure fields for a homogeneous atmosphere, indicating a correct implementation of the simplified ray model.

6.4 Hybrid Model validation

The first stage of the validation process was the determination of suitable limits γ_{bottom} and γ_{top} to apply equation (25).

This procedure consisted on the computation of the pressure field in a homogeneous atmosphere along four different downward travelling lines with elevation angles of $30°$, $40°$, $50°$ and $60°$.

The results obtained following this analysis suggest that limiting the merging zone between elevation angles of $40°$ and $50°$ is the more appropriate choice and therefore the validation of the hybrid model (test case 6) adopted this limiting angles.

Figure 3 plots the pressure field in the conditions of case 6 using the three propagation models described in this text.

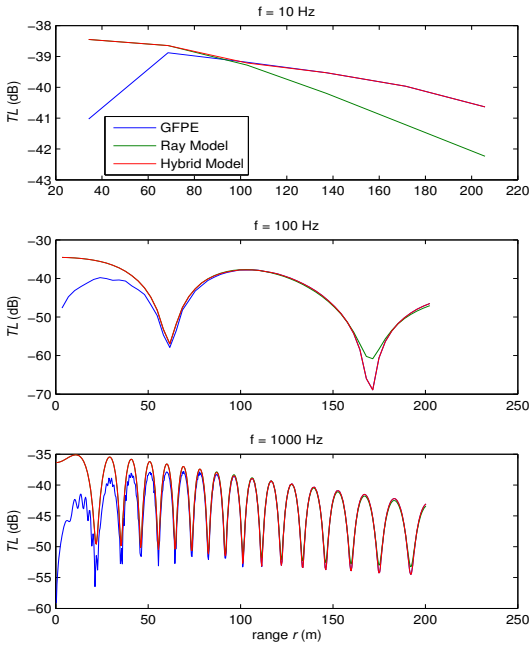

Figure 3 - Transmission loss as a function of range using the GFPE method, the ray model and the hybrid model, for test case 6.

From this figure we may verify that the hybrid model provides a smooth transition between the GFPE method and the two ray model for the entire frequency interval tested. We may detect that the hybrid model follows equation (25) because for short ranges, i.e. high elevation angles, the obtained function is indistinguishable from the ray model while for longer ranges the curve is coincident with the one related to the GFPE method.

For non-refracting atmospheres, the hybrid model exhibits similar behaviors, although for higher frequencies some oscillations may be observed in the merging region. Despite this phenomenon, the accuracy of the results is still preserved as the variation of the transmission loss in the transition region is small.

Therefore, we implemented the merging region using the proposed limiting angles.

7 Aviation noise near an airport

To study the adequacy of the hybrid propagation model in an airport scenario, we simulated different aircraft trajectories based on the Airbus A320 at Lisbon airport. The first simulated trajectory was based on an ILS approach and the receiver was placed $2km$ before the runway and aligned with the runway's centerline. We were able to obtain the following results regarding the sound exposure level (SEL), which were compared with the experimental data published by Correia (2011) as presented in Table 5.

Table 5 - SEL from numerical calculations and experimental measurements for the ILS approach.

Experimental	Numerical	Deviation
$90.99\ dB$	$88.3\ dB$	$2.69\ dB$

From Table 5, we may conclude that the numerical methods produce coherent results with the experimental data, as the relative deviation between both sets of values is acceptable.

Table 6 - Definition of the takeoff stages (in feet AGL) for the departure trajectories.

	Case 1	Case 2	Case 3	Case 4	Case 5
Thrust Reduction	800	800	1000	1500	1500
Flap Retraction	1500	800	1000	1500	3000
Acceleration	3000	3000	2500	1500	3000

Table 7 - SEL (dB) for the reviewed departing procedures and for each receiver position.

	Case 1	Case 2	Case 3	Case 4	Case 5
Receiver 1	85.7	86.2	86	86	85.5
Receiver 2	87.6	88.5	88.1	90.2	90.5

The second set of results obtained with the numerical program consisted of five noise reduction procedures for departing flights (International Civil Aviation Organization, 2007). The procedures followed common guidelines and are characterized by three separate actions (see Table 6), which produce the trajectories shown in Figure 4.

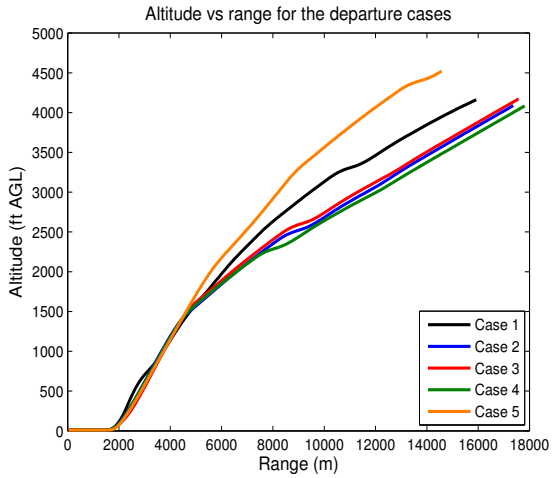

Figure 4 - Altitude as function of distance to the start of takeoff roll.

Table 7 presents the SEL results for two different receivers, the first one located at a distance of $6.5\,km$ from the beginning of the takeoff roll and aligned with the runway centerline extension and the other placed at a distance of $5\,km$. From the numerical results, we may conclude that noise reduction trajectories are related to the region where sound levels are to be mitigated. Additionally, the results suggest that, in order to minimize the impact of departing aircraft near the airport, engine thrust should be reduced to climb setting before reaching the observer. On the other hand, when reducing the noise indices in regions that are far from the runway, it can be verified that the aircraft should adopt a trajectory that increases the minimum distance between the airplane and the receiver and consequently the power cutback action may be delayed to allow a longer climb segment at a higher climb gradient.

8 Conclusions

In this text we developed a noise prediction program oriented towards aviation noise in the vicinity of airports using Matlab programming language. This computational tool includes not only physics-based atmospheric propagation methods but also adopts empirical models that allow the definition of aircraft as complex noise sources.

The numerical schemes used to calculate sound propagation in the atmosphere were the Green's Function Parabolic Equation (GFPE) method and the two ray model. These methods were combined into a hybrid model in order to mitigate their limitations and maximize their potential.

The propagation methods were validated using benchmark test cases that are accepted as a standard in the verification of atmospheric sound propagation models. The adopted procedure involved three different stages, namely the validation of the GFPE method, the verification of the simplified ray model and the definition of the

transition region. The similarity between the results from the implemented methods and the reference data allowed the validation of the numerical implementation process.

At last we discussed the application of the hybrid propagation model to an airport scenario by resorting to realistic flight conditions in two different stages. In the first part, we studied an approach simulation to Lisbon airport. The results obtained from the landing simulation were compared with published experimental results and the agreement between the numerical values and the experimental data confirmed the adequacy of the program to real aircraft operations. In the last stage, we simulated a set of five noise reduction techniques for takeoffs that are typically used by airlines. The results obtained with these trajectories indicated that noise abatement procedures should be chosen according to the region where sound levels are to be minimized. Therefore, for receivers closer to the airport, thrust reduction should be accomplished before reaching the observer, while for regions far from the runway the initial climb segment, which is characterized by a steeper climb gradient, should be extended to allow the maximization of the distance between the aircraft and the observer.

Despite the results obtained with the model proposed in this dissertation, it should be kept in mind that multiple simplifications were considered. To achieve a more realistic description of the environment in the vicinity of airports, future developments should include more complex models considering atmospheric turbulence as well as a more realistic definition of the ground surface simulating noise barriers, topographic features and different ground materials representing normalized impedances discontinuities. Additionally, aircraft dynamics may be included in the program to allow the implementation of optimization tools as a means of obtaining a realistic flight path with minimum noise impact.

9 References

Attenborough, K., Taherzadeh, S., Bass, H. E., Di, X., Raspet, R., Becker, G. R., Gudesen, A., et al. (**1995**). “Benchmark cases for outdoor sound propagation models,” J. Acoust. Soc. Am., **97**, 173–191.

Boeker, E., and Rosenbaum, J. E. (**2012**). “Intelligent switching between different noise propagation algorithms : analysis and sensitivity,” INTERNOISE 2012,.

Butikofer, R. (**2006**). *IMAGINE -Default aircraft source description and methods to assess source data*, IMAGINE project.

Cooper, J. L., and Swanson, D. C. (**2007**). “Parameter selection in the Green’s function parabolic equation,” Appl. Acoust., **68**, 390–402.

Correia, G. S. D. (**2011**). *Previsão de níveis de ruído aeronáutico na vizinhança do Aeroporto de Lisboa* , M. Sc. Thesis, Instituto Superior Técnico.

Eurocontrol (**2012**). *Aircraft Noise and Performance (ANP) database*, Available: http://www.aircraftnoisemodel.org. Retrieved from http://www.aircraftnoisemodel.org

Gilbert, K. E., and Di, X. (**1993**). “A fast Green’s function method for one-way sound propagation in the atmosphere,” J. Acoust. Soc. Am., **94**, 2343–2352.

International Civil Aviation Organization (**2005**). *Annex 16 to the convention on international civil aviation: Environmental Protection, Volume I: Aircraft Noise*, ICAO.

International Civil Aviation Organization (**2007**). *Review of noise abatement procedure research & development and implementation results*, ICAO.

International Civil Aviation Organization (**2010**). *Environmental Report 2010*, ICAO.

Salomons, E. M. (**2001**). *Computational Atmospheric Acoustics*, Kluwer Academic Publishers.

Society of Automotive Engineers (**2006**). *SAE Aerospace Information Report, “AIR 5662: Method for Predicting Lateral Attenuation of Airplane Noise,”* SAE International.